Vrije Universiteit Brussel

VUB VRIJE UNIVERSITEIT BRUSSEL

Fine scale measurements in Belgian coastal sediments reveal different mobilization mechanisms for cationic trace metals and oxyanions

Gao, Yue; Zhou, Chunyang; Gaulier, Camille; Luo, Mingyue; Guo, Wei; Baeyens, Willy

Link to publication

Download date: 20. Apr. 2024

ELSEVIER

Fine scale measurements in Belgian coastal sediments reveal different mobilization mechanisms for cationic trace metals and oxyanions

Chunyang Zhou [a], Camille Gaulier [a,c], Mingyue Luo [a], Wei Guo [b], Willy Baeyens [a], Yue Gao [a,*]

[a] Analytical, Environmental and Geo-Chemistry Department (AMGC), Vrije Universiteit Brussel (VUB), Pleinlaan 2, 1050 Brussels, Belgium
[b] College of Architecture and Civil Engineering, Beijing University of Technology, Beijing 100124, China
[c] LASIR CNRS UMR 8516, Universite de Lille, Cite Scientifique, 59655 Villeneuve d'Ascq Cedex, France

ABSTRACT

Belgian coastal sediment serves as an important sink for trace elements, yet a systematic study covering a wide range of elements including redox-sensitive metals (Fe, Mn, and Co), cationic trace metals (Cd, Pb, Ni, Cu, and Zn), oxyanions (P, V, As, and Mo), and sulfide has not been performed and the mechanisms controlling their mobilization were not investigated. Here, a passive sampling technique, Diffusive Gradients in Thin-films (DGT), was used *in situ* to obtain high resolution concentration profiles of these elements in the sediment porewater. Our results revealed two mobilization mechanisms of cationic trace metals and oxyanions in Belgian coastal sediments, both strongly linked to the cycling of Fe. Mobilization of Co, Pb, Ni, and Cu is controlled by electrogenic sulfur oxidation, acidification of the porewater and dissolution of FeS, while that of oxyanions (P, V, and As) is controlled by reductive dissolution of Fe oxyhydroxides. Constant cationic trace metal to Fe molar ratios were established in FeS, while the oxyanion to Fe ratios in Fe oxyhydroxides differ significantly between sampling stations, which is primarily caused by competing effects. We found no evidence that cationic trace metal mobilization was related to Fe oxyhydroxides, or oxyanion mobilization to FeS. This suggests that particulate organic matter forms the major pathway for cationic trace metal input in coastal sediments and that oxyanions will not be incorporated in FeS but form their own oxyanion-sulfide compound. These findings will contribute to a better understanding of the mobilization mechanisms of cationic trace metals and oxyanions in coastal sediments, and of their biogeochemical cycling in coastal ecosystems.

1. Introduction

Iron (Fe), manganese (Mn), and trace elements play important roles in regulating ocean processes including phytoplankton growth and carbon cycling (Baeyens et al., 2018; Morel et al., 1994). The role of Fe, Mn, and Cu in the surface ocean is well known as they are essential micronutrients. Their availability influences the physiological state and biochemical activity of marine organisms (Morel and Price, 2003). Several trace metals (e.g., Co, Cd, Ni, Zn) act as limiting or co-limiting micronutrients to diatom growth as they are involved in metabolic processes, such as carbon dioxide acquisition and silica uptake (Morel et al., 2006). Other trace elements (e.g., V, Mo), also known as oxyanions, are identified in many metalloenzymes and proteins, including nitrate reductases (Antipov et al., 1999; Maia and Moura, 2015) and nitrogenases (Eady, 2003; Rehder, 2000), which have essential functions in processes like nitrogen fixation and nitrate assimilation

(Howarth and Cole, 1985; Wang and Sañudo Wilhelmy, 2009). Lead (Pb) and arsenic (As) are known to be toxic contaminants which can strongly influence the dynamics of phytoplankton communities (Morel et al., 2006). Thus, understanding the biogeochemical cycling of these elements becomes important for a better protection of the marine ecosystem.

Marine sediments act as both a source and a sink of Fe, Mn, and trace elements, and thus influence the concentrations and distributions of these elements in the water column, depending on the local bottom conditions, sediment resuspension activity, and the local geochemical cycling regime in the sediment (Sullivan and Aller, 1996). Trace elements enter sediment mainly in particulate form. Some metals (e.g., Cd, Cu, Ni) are principally adsorbed onto organic matter (Gendron et al., 1986; Johnson et al., 1988), while others (e.g., Co, As, Pb) are typically associated with iron and manganese oxyhydroxides (Gendron et al., 1986; Kay et al., 2001; Stockdale et al., 2010b). Early diagenesis results

* Corresponding author.
  E-mail address: yue.gao@vub.be (Y. Gao).

in geochemical transformation of these particles as soon as they are deposited at the bottom. Organic matter is mineralized by heterotrophic microorganisms resulting in production of carbon dioxide and consumption of oxidants. This process is controlled by several parameters, mainly the quantity and quality of organic matter, temperature, and the availability of oxidants (oxygen, nitrate, oxyhydroxides of iron and manganese, and sulfate) which are consumed by the different bacterial populations (Berner, 1980). As a side effect of the degradation of organic matter and the dissolution of Fe and Mn oxyhydroxides, trace elements are released into porewater. However, other geochemical processes will disturb this straightforward transfer of trace elements from the solid to the dissolved phase. The reduction of sulfate into sulfide results in the precipitation of numerous elements like Fe, Pb, Zn, Cu, or As (Borch et al., 2006; Canavan et al., 2007). Other dissolved trace elements will diffuse towards the surface sediment and are re-captured by iron and manganese oxyhydroxides when passing through the oxic layer at the sediment–water interface (SWI). The geochemical cycling of Fe, Mn, and trace elements in the sediment is thus controlled by mineralization and oxidation/reduction processes.

In coastal areas, the pressure exerted by natural processes and anthropogenic activities on the ecosystem makes geochemical cycling of Fe, Mn, and trace elements in the sediment more complex. For example, high amounts of endogenous and terrestrial organic matter from the nearby coast can increase the heterotrophic activity in surface sediments, and thus increase the organic carbon mineralization rate which may potentially promote Fe, Mn, and trace element remobilization in sediments (van de Velde et al., 2018). Meanwhile, tidal currents, wave action, and activities including dredging and bottom trawling can relocate and redistribute upper sediment layers, and thus influence the redox pathways of organic matter mineralization which may reduce the burial efficiency of these elements in sediments (Halpern et al., 2008; Lohrer and Wetz, 2003). The Belgian coastal zone (BCZ) is a shallow coastal area, where the surface sediment is mixed by tidal cycles and enriched in organic matter and carbonate, with a shallow oxygen penetration depth of 1 to 3 mm (van de Velde et al., 2016). Frequent anthropogenic disturbance keeps the geochemistry of the coastal seafloor in a transient, fast-changing state, resulting in accelerated cycling of Fe, Mn, and trace elements in the BCZ sediment which imposes a potential threat to both benthic and water column organisms.

Several studies have been carried out in the BCZ sediments and understanding of Fe, Mn, and trace element cycling in those sediments is improving in line with technological progress (Gao et al., 2019, 2012, 2009). The passive sampling technique Diffusive Gradients in Thin-films (DGT) (Davison and Zhang, 1994) provides fine scale (sub-mm) profiles of Fe, Mn, and trace elements in sediment porewater with minimum disturbance, allowing to investigate small scale mobilization mechanisms (Gao et al., 2015; Zhou et al., 2018). However, until now, geochemical studies in the BCZ did not consider oxyanions like V, As, and Mo. These oxyanions possess some similar characteristics to phosphate (Stockdale et al., 2010a), the major nutrient controlling phytoplankton growth in the BCZ water column (Muylaert et al., 2006). The DGT technique using zirconium oxide (ZrO) resin can simultaneously measure P, V, Mo, and As in different environments including sediment (Guan et al., 2015). This ZrO DGT together with Chelex-100 and silver iodide (AgI) DGTs, which are respectively used for the measurement of cationic metals (Zhang et al., 1995; Zhou et al., 2018), and dissolved sulfide (Teasdale et al., 1999) which is a major factor influencing immobilization/mobilization of Fe, Mn, and trace elements, provides an opportunity to perform a comprehensive study of geochemical cycling of a wide range of elements in the BCZ sediment.

In this study, three groups of elements are investigated. Fe, Mn, and Co are redox-sensitive metals as they have several stable oxidation states and their behavior is closely related to redox reactions in oxic/anoxic sediments (Thamdrup et al., 1994). Cd, Pb, Ni, Cu, and Zn belong to cationic trace metals (Co may also be included here), which are normally not involved in redox reactions, but form complexes with organic ligands or dissolved anions and are easily scavenged by particles like organic matter and Fe/Mn oxyhydroxides (Morel and Price, 2003). P, V, Mo, and As are oxyanions and efficiently adsorb onto Fe/Mn oxyhydroxides in aqueous solution. The oxygen atoms in the oxyanion complex can be replaced by sulfide which leads to the formation of thiol-complexes and concomitant changes in adsorption properties (Emerson and Huested, 1991; Gustafsson, 2003). The aim of our study is to investigate fine scale mobilization mechanisms of redox-sensitive metals, cationic trace metals, oxyanions, and sulfide in the BCZ sediment by using DGT technique, and thus to improve our understanding of geochemical cycling of these elements in Belgian coastal ecosystem.

2. Material and methods

2.1. Sampling stations and sediment core collection

Two sampling stations in the Belgian coastal zone (BCZ), W1 and W2, are selected (Figure S1). Station W1 (51°21′45″N, 3°11′39″E) is located close to the Zeebrugge harbor and is around 3 km away from the coastal line. Station W2 (51°15′20″N, 2°51′22″E) is located close to the Oostende harbor and is around 4.5 km away from the coastal line. The distance between the two stations is around 25.7 km. Stations W1 and W2 (Figure S1) have similar water depths (around 10 m) and have been exposed for several decades to high human pressure as a result of a dense population (~352 inhabitants per km^2) and of industrial (petrochemical and oil refinery plants) and agricultural activities (Gao et al., 2013; van de Velde et al., 2018). Three sediment cores with around 5 cm overlying water were collected at each station by reineck box corer on the RV Simon Stevin (a research vessel served for Flanders Marine Institute) in October 2019. Sediment cores were carefully transported back to the lab immediately after collection. They were then incubated separately in two tanks filled with sea water (~50 L) collected from the corresponding station. The overlying water of the sediment core was kept oxygenated by continuously bubbling air in each tank (van de Velde et al., 2017) to mimic the *in situ* conditions. One of the cores was used for pH and redox potential measurements. In the other two cores DGT probes were inserted.

2.2. Measurement of redox potential and pH in sediment core

Measurement of redox potential was performed using a redox electrode (SCHOTT Pt 62) with an Ag/AgCl reference system. Measurement of pH was performed using a pH electrode (pHenomenal 110) with the same reference system. All electrodes were calibrated before the application. Redox potential and pH were measured first in the overlying water and then in the sediment core at 2 cm intervals.

2.3. DGT probe preparation

A DGT probe is a rectangular, plastic moulding which consists of a base overlaid sequentially by a resin gel layer (0.4 mm thickness), a diffusive gel layer (0.8 mm thickness), a filter membrane (0.125 mm thickness, PVDF), and covered by a cap with a window area of 150×18 mm (length × width). Three types of DGT probes were used in this study, a ground Chelex-100 (GCH) probe for metal cation determination, a zirconium oxide (ZrO) probe for oxyanion determination, and a silver iodide (AgI) probe for sulfide determination. GCH resin gel was prepared according to Zhou et al. (2018), ZrO resin gel was prepared according to Guan et al. (2015), and AgI resin gel was prepared according to Gao et al. (2015). Diffusive gel preparation and DGT probe assembly can be found elsewhere (Gao et al., 2015).

Prior to deployment, DGT probes were deoxygenated in 0.1 M NaCl solution overnight with continuous bubbling of N_2 gas.

2.4. DGT probe deployment and retrieval

DGT probes were vertically inserted into the sediment cores with caution to ensure minimum disturbance, leaving around 2 cm of the window area of the probe above the SWI. For each station, a GCH probe and a ZrO probe were arranged back to back and inserted into one sediment core for 12 h, and a AgI probe was deployed in a separate core for 8 h. After deployment, DGT probes were retrieved and the window area exposed to the sediment was thoroughly rinsed with MQ water. After cleaning, the resin gels were peeled from the probes and treated as described below.

2.5. Sample treatment

2.5.1. GCH resin gel treatment and analysis

GCH resin gel was sliced at 0.5 cm interval. Each slice was then eluted with 1 mL 1 M HNO_3 for 24 h and the eluate samples were diluted 10 times with MQ water before ICP-MS measurement.

2.5.2. ZrO resin gel treatment and analysis

ZrO resin gel was sliced in the same manner as GCH resin gel. Each slice was then eluted with 3 mL 0.5 M NaOH for 24 h and the eluate samples were diluted 10 times with 0.15 M HNO_3 before ICP-MS measurement.

2.5.3. AgI resin gel treatment and analysis

AgI resin gel was treated differently from the other two resin gels. Firstly, the water layer on the surface of the gel was carefully removed with dust-free paper (Kimtech®). The gel was then placed between two transparent plastic membranes followed by a surface scanning in grey-scale mode using a flat-bed scanner (HP 3100). The color change of the gel from pale yellow to dark brown is due to the formation of AgS. The scanned greyscale image was then processed by Fiji software (Fiji is an open source image processing package based on ImageJ) and the concentration of dissolved sulfide was calculated using the calibration curve in Figure S2. Details relating to the calibration curve are reported in supplementary material. 1D depth profiles of dissolved sulfide were obtained by averaging 2D images over the horizontal dimension.

2.6. Data analysis

The DGT results were interpreted as DGT concentrations by using the following equation (1):

$$C_{DGT} = \frac{M \times \Delta g}{D \times A \times t} \tag{1}$$

Where M is the accumulated mass (ng) of the target analyte on the resin gel, Δg is thickness (cm) of diffusive layer (diffusive gel + filter), D is the diffusion coefficient ($cm^2 \, s^{-1}$) of the target analyte in the diffusive layer (values are available at https://www.dgtresearch.com/diffusion-coefficients/), A is the exposed area (cm^2) of the gel to the sediment and t is the deployment time (s). The DGT technique does not measure the real labile analyte concentration in porewater. It effectively measures an interaction between the initial labile concentration in porewater and resupply from the solid phase to porewater upon perturbation by a local sink, such as the DGT device. Therefore, concentrations measured by DGT can be interpreted as a combination of actual labile concentrations increased by local resupply (Arsic et al., 2018; Zhang et al., 2002). Hereinafter, the element concentrations in the text refer to DGT concentrations if there is no specific indication.

The Person method was used to evaluate the significance of correlation between different elements at significance levels of 0.05 and 0.01 (Sigmaplot 14.0, Systat Software Inc.). QA/QC information is reported in the supplementary material.

3. Results

3.1. Redox potential and pH profiles in the BCZ sediment

Redox potential and pH profiles in the BCZ sediments are shown in Fig. 1. A clear drop of redox potential at SWI zone (between 2 cm and −2 cm) was observed for both stations (W1 and W2). At station W1, the redox potential decreased from 120 mV in the overlying water to −240 mV at −2 cm depth followed by a smooth decline to −340 mV at −10 cm depth and a slight increase till the bottom. At station W2, the redox potential dropped from 220 mV in the overlying water to −93 mV at −2 cm depth with a smooth decrease till the bottom. A decrease of pH from overlying water to the bottom of the sediment core was found at both stations. The pH dropped from 7.5 to 7.1 at station W1, and from 7.7 to 7.2 at station W2. Similar redox potential and pH profiles in the BCZ sediment were reported in literature (Gao et al., 2009; Gillan et al., 2012).

3.2. Fine scale mobilization of redox-sensitive metals, cationic trace metals, and oxyanions in the BCZ sediment

3.2.1. Redox-sensitive metals (Fe, Mn, and Co)

Vertical DGT concentration profiles of Fe, Mn, and Co in the W1 sediment are shown in Fig. 2. Substantial remobilization of Fe was observed below the SWI resulting in a broad concentration maximum between 0 to −6 cm depth (highlighted in blue in Fig. 2). The highest concentration of 41 µM was found at −3 cm depth. A small increase of Fe was also discovered after −9 cm depth till the bottom with a concentration reaching 25 µM (highlighted in grey in Fig. 2). Substantial remobilization of Mn was also observed in the sediment with concentrations staying around 25 µM between 0 to −6 cm depth and a small maximum of 30 µM at −8 cm. However, different from Fe, there was no distinct removal process at SWI resulting in Mn concentrations in the overlying water similar as those below the SWI. It is commonly recognized that once dissolved Fe produced in the sub-oxic sediment layer diffuses upwards to the oxic interface layer, it will be quickly oxidized forming insoluble Fe oxyhydroxides. However, this oxidation and removal process for Mn is much slower than for Fe (Lourino-Cabana et al., 2014). A slight drop of Mn was found after −8 cm depth till the bottom, which is opposite to the increasing trend of Fe at the same depth. From surface to −8 cm depth, Co stayed close to zero without any clear increase, while from −8 cm to bottom, it increased to 6.8 nM, similar to Fe.

The general pattern of DGT concentration profiles of Fe, Mn, and Co
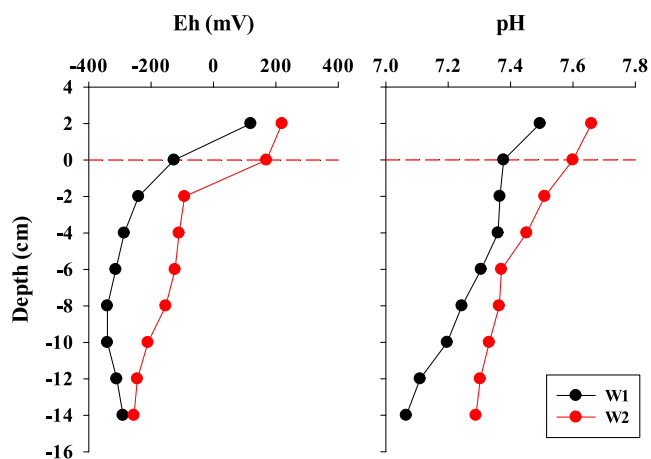

Fig. 1. Redox potential (Eh) and pH profiles in the sediments at stations W1 and W2 (red dashed line represents the sediment–water interface). (For interpretation of the references to color in this figure legend, the reader is referred to the web version of this article.)
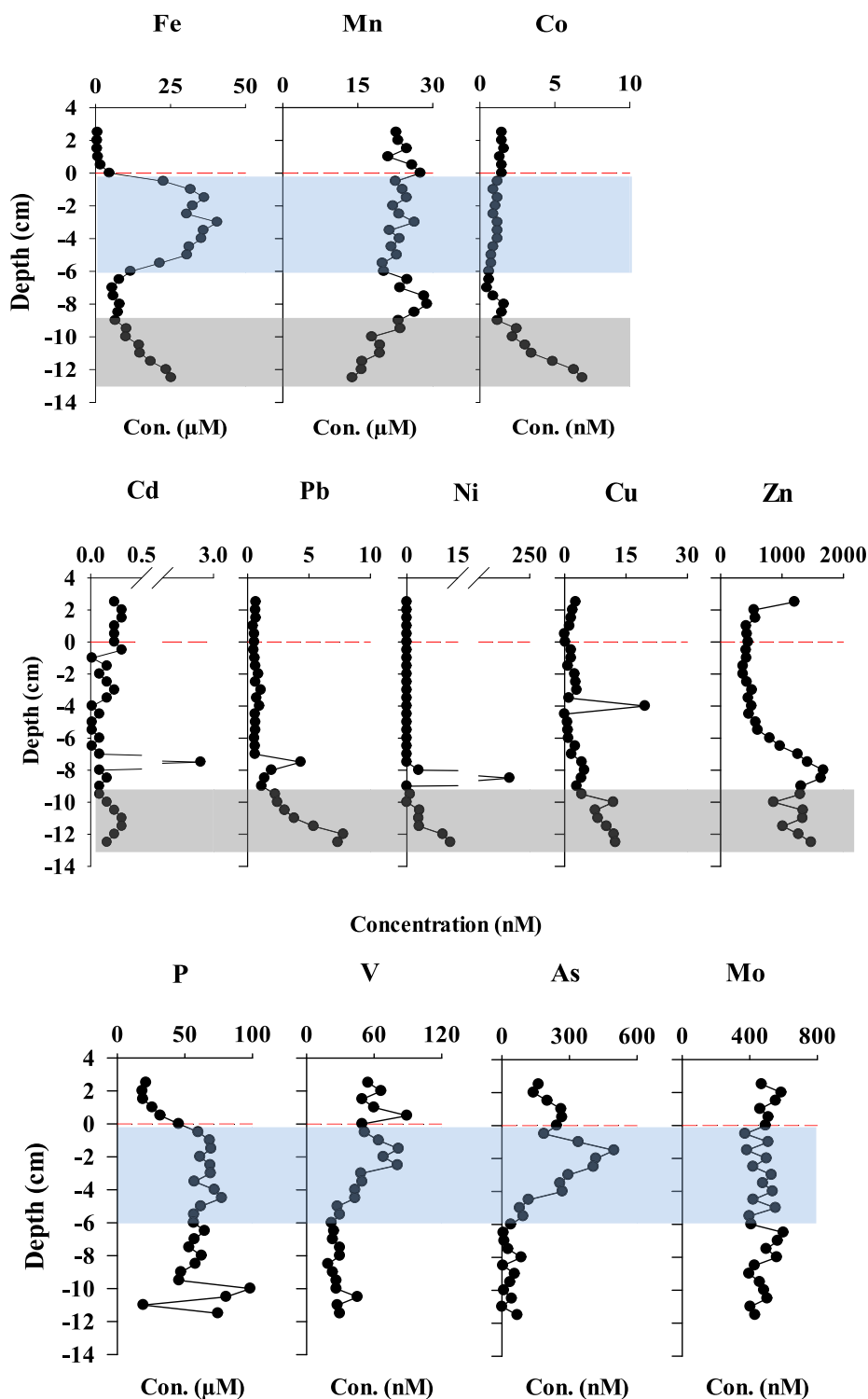
Fig. 2. DGT concentration profiles of redox-sensitive metals (Fe, Mn, and Co), cationic trace metals (Cd, Pb, Ni, Cu, and Zn), and oxyanions (P, V, As, and Mo) in the sediment at station W1 (red dashed line represents the sediment–water interface, the blue zone ranges from 0 to −6 cm depth, the grey zone ranges from −9 to −12.5 cm depth). (For interpretation of the references to color in this figure legend, the reader is referred to the web version of this article.)

in the sediment at station W2 is similar to that in the sediment at W1 but the details differ (Fig. 3). In brief, Fe showed a sharp peak at −2.5 cm depth with the concentration reaching 35 μM (highlighted in blue in Fig. 3) and a small increase after −9 cm till the bottom (highlighted in grey in Fig. 3), while Mn was smoothly decreasing from 20 μM at SWI to 10 μM at the bottom.. A clear drop of Co from 1.9 to 0.7 nM was found at −1 cm depth. It then stayed close to zero between −2 and −9 cm depth,

followed by a sharp increase till the bottom, similar to Fe.

3.2.2. Cationic trace metals (Cd, Pb, Ni, Cu, and Zn)

DGT concentration profiles of Cd, Pb, Ni, Cu, and Zn in W1 sediment are shown in Fig. 2. Pb, Ni, and Cu showed similar profiles as their concentrations were low from overlying water to −9 cm depth, followed by an obvious increase where Fe was also increasing. Besides that, Ni
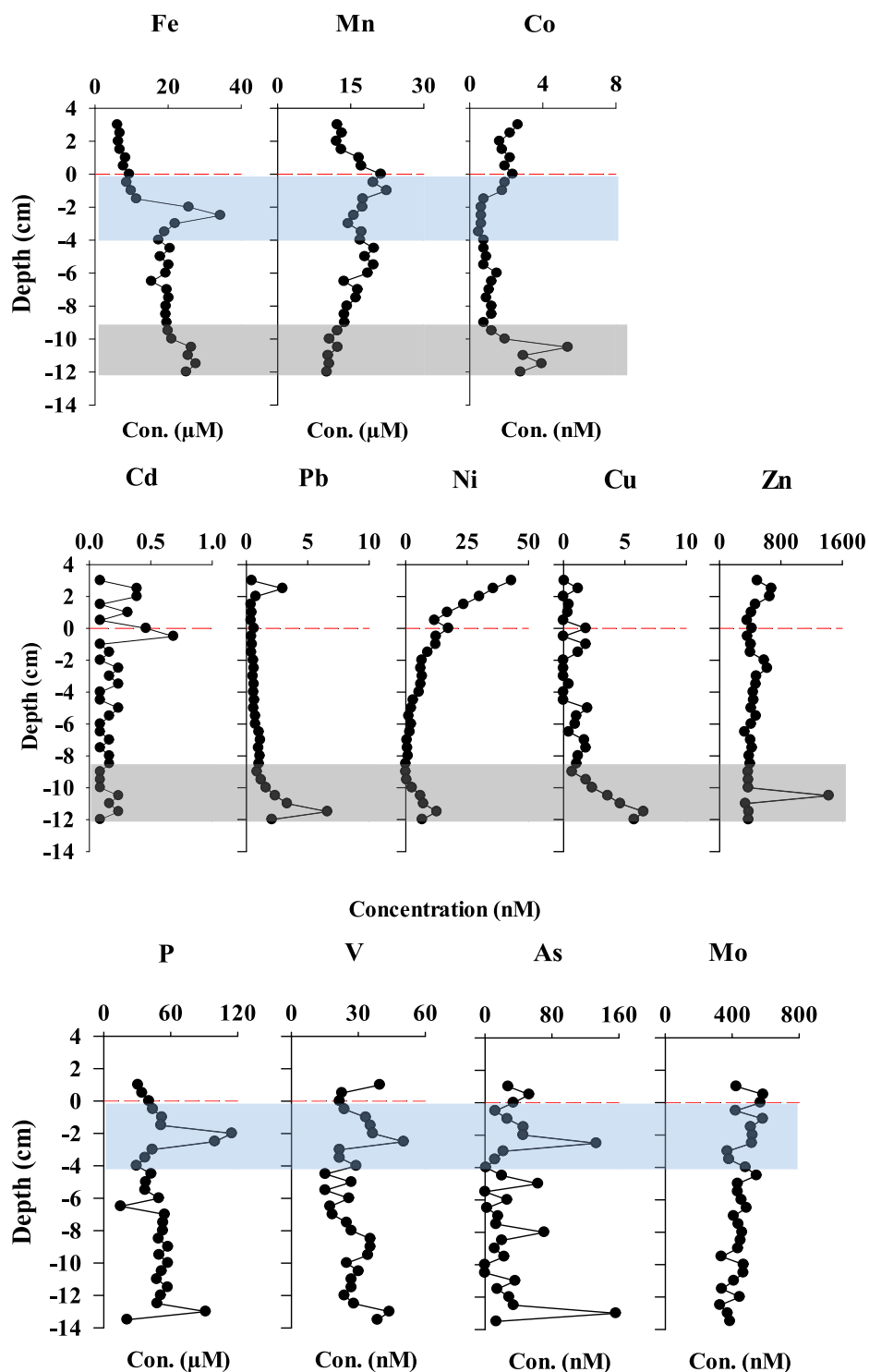
Fig. 3. DGT concentration profiles of redox-sensitive metals (Fe, Mn, and Co), cationic trace metals (Cd, Pb, Ni, Cu, and Zn), and oxyanions (P, V, As, and Mo) in the sediment at station W2 (red dashed line represents the sediment–water interface, the blue zone ranges from 0 to −4 cm depth, the grey zone ranges from −9 to −12 cm depth). (For interpretation of the references to color in this figure legend, the reader is referred to the web version of this article.)

peaked at −8.5 cm depth with a concentration reaching 210 nM and Cu peaked at −4 cm depth with a concentration up to 20 nM. The peak of Pb (4.3 nM) coincided with that of Cd (2.9 nM) at −7.5 cm depth. Zn concentration (above 300 nM) was much higher than other trace metals and Zn profile started to increase at shallower depth (-6 cm) than other trace metals, with a peak of 1700 nM at −8.5 cm depth. At greater depth, Zn was fluctuating around 1000 nM.

Similar to the observation at station W1, DGT concentration profiles of Pb, Ni, and Cu at station W2 (Fig. 3) showed a clear increase from −9 cm depth till the bottom. An obvious concentration decrease of Ni was found when entering the sediment, indicating a significant influx of Ni from overlying water to sediment. A prominent peak of Zn was found at −10.5 cm depth with a concentration reaching 1400 nM. Cd concentration fluctuated in the entire sediment core with a small peak of 0.7 nM

right below the SWI.

For various metals a few sharp peaks, defined by a single concentration point, are noticed (Figs. 2 and 3). Previous work at such small-scale resolution (5 mm) has shown similar features (Gao et al., 2009; Leermakers et al., 2005), but at higher resolution (100 μm) and in 2D highly localized mobilization areas could be observed (Gao et al., 2015; Stockdale et al., 2009). However, it is only possible to make such measurements at high resolution and in 2D over a limited area of the DGT binding layer. The resolution used here involved a much larger spatial scale and does not permit detailed analysis and interpretation of these single sharp peaks.

3.2.3. Oxyanions (P, V, As, and Mo)

DGT concentration profiles of P, V, As, and Mo in W1 sediment are shown in Fig. 2. A clear concentration increase was found for P starting from 1 cm in the overlying water to −2 cm in the sediment. The concentration then stayed around 70 μM till −9 cm depth followed by more fluctuations close to the bottom of the core. Similar profiles were noticed for V and As which had a coincident concentration maximum between 0 and −6 cm depth, where Fe was also substantially released. After −6 cm depth, V and As were close to zero till the bottom. Mo stayed around 500 nM in the entire sediment core including the overlying water without any clear maximum/minimum. A possible explanation is that the mobilization of Mo is highly associated with Mn, whose profile also showed minor variation. Mn oxyhydroxide particles are commonly considered as major carrier phases of Mo in the water column and the deposition of these particles dominates the input of Mo to the sediment (Scholz et al., 2013). Mo enrichment associated with Mn oxyhydroxides near the SWI was found in many coastal areas (Scholz et al., 2013; Sulu-Gambari et al., 2017).

DGT concentration profiles of oxyanions in W2 sediment are shown in Fig. 3. A coincident maximum was found for P, V, and As at −2.5 cm depth with concentrations reaching 120 μM, 50 nM, and 130 nM respectively. Moreover, it corresponds to the peak of Fe at the same depth. Another coincident maximum of P, V, and As was found at −13 cm depth with concentrations reaching 90 μM, 45 nM, and 160 nM respectively. It is clear that the mobilization of P, V, and As in W2 sediment are highly associated. Similar as the profile at station W1, Mo showed a relatively constant profile at station W2 with concentrations staying around 500 nM.

3.3. Fine scale mobilization of sulfide in the BCZ sediment

DGT concentration profiles of sulfide and Fe at stations W1 and W2 are shown in Fig. 4. At station W1, the concentration of sulfide started to increase at around −9 cm depth which coincides with the increase of Fe. A clear peak of sulfide was observed at −12 cm depth with a

concentration reaching 56 μM. At station W2, sulfide started to increase at −4 cm depth with a concentration peak of 100 μM observed at −6.5 cm depth. The fact that sulfide started to increase at shallower depth at station W2 than at station W1 might be due to the lower amount of Fe oxyhydroxides, a stronger oxidant than sulfate, at station W2. In sediment, Fe/Mn oxyhydroxides are reduced prior to sulfate reduction. At station W1, it appears that Fe was strongly removed from porewater at −6 cm depth where sulfide was absent. This suggests that Fe was not removed by precipitation with sulfide. Other possibilities for the decrease of Fe include: (1) precipitation of Fe(II) as carbonates, supported by the observed iron carbonates in the BCZ surface sediment (van de Velde et al., 2017); (2) oxidation of Fe(II) by available oxidants (e.g., nitrate, Mn oxides) (Robertson et al., 2016); (3) complexation of Fe(II) with organic ligands that are not labile or might be too large to enter the DGT device (Gao et al., 2019). Further investigation is required to verify those possibilities. Similar DGT concentration profiles of Fe and sulfide in the BCZ sediment have been reported in other studies (Gao et al., 2009; Lourino-Cabana et al., 2014).

4. Discussion

In oxic conditions, Fe and Mn form insoluble oxyhydroxides which act as major carrier phases for cationic trace metals and oxyanions in both water column and sediment. In sub-oxic conditions, Fe and Mn oxyhydroxides are reduced and dissolved, releasing associated elements at the same time. In anoxic conditions, sulfate reduction dominates and the produced sulfide will remove these elements from sediment porewater by (co)precipitation. Overlying water at stations W1 and W2 was oxic, but once crossing the SWI the redox conditions changed to sub-oxic and to anoxic at greater depth (Figs. 1 and 4). These redox shifts will inevitably exert influences on the cycling of a wide range of elements in sediments, directly on the redox sensitive ones (e.g., Fe, Mn, and sulfide) and indirectly on the non-redox ones (e.g., Pb, Ni, Cu and P). This first study of fine scale (5 mm and 0.05 mm for sulfide) mobilization of a suite of elements in the BCZ sediments (Figs. 2, 3, and 4) using DGT has revealed different mobilization mechanisms for the 3 groups of elements (redox-sensitive, cationic trace metals, and oxyanions), as discussed below.

4.1. Co-mobilization of Pb, Ni, Cu, and Co with Fe in the BCZ sediment

Two distinct remobilization zones of Fe were discovered in both W1 and W2 sediments. As shown in Figs. 2 and 3, these two zones are highlighted in blue and grey. The simultaneous release of Co/Pb/Ni/Cu and Fe was found in the grey zones at both stations, while Cd, Zn, and the oxyanions showed less association with Fe in this zone. Correlation analysis indicated that cationic trace metals (Co, Pb, Ni, and Cu) are significantly correlated ($p < 0.05$) with Fe in the grey zones at both stations (Fig. 5). The most significant correlation was found between Co and Fe at station W1 ($R^2 = 0.99$), and between Ni/Cu and Fe at station W2 ($R^2 = 0.84$). The concurrent release of cationic trace metals and Fe is commonly attributed to the dissolution of Fe oxyhydroxides. However, this mostly happens close to the sediment surface where Fe oxyhydroxides are fresh and abundant (Fones et al., 2004). If Fe oxyhydroxides were reduced in the deeper grey zone, the liberated Fe would react with S(-II) and so dissolved Fe would not be measurable. A possible reason for increased Fe concentrations in the grey zone is that there exists a process responsible for dissolution of FeS in anoxic conditions. The fact that Fe and sulfide were simultaneously increasing in this zone supports such process. It is worth noting that sulfide increased to 50 μM which was 2.5 times higher than the rise of Fe (20 μM) in this zone. This is reasonable as sulfate reducing bacteria produce continuously sulfide that can reach much higher levels than those of Fe, the major cation with which it will precipitate. Therefore, Fe and sulfide should not be stoichiometrically in equilibrium, even if dissolution of FeS is the source of increased Fe concentrations in the grey zone. During FeS precipitation,
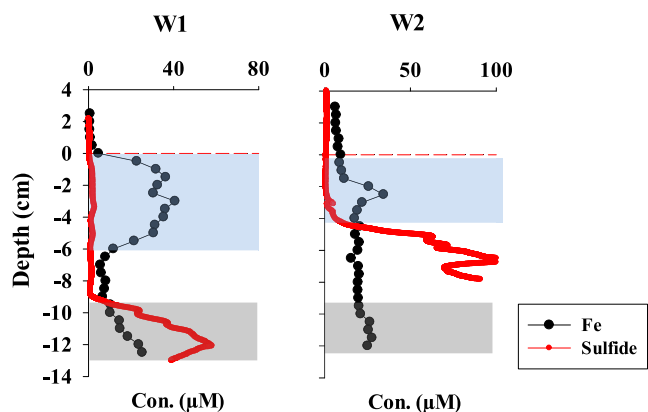

Fig. 4. DGT concentration profiles of Fe and sulfide in the sediments at stations W1 and W2.
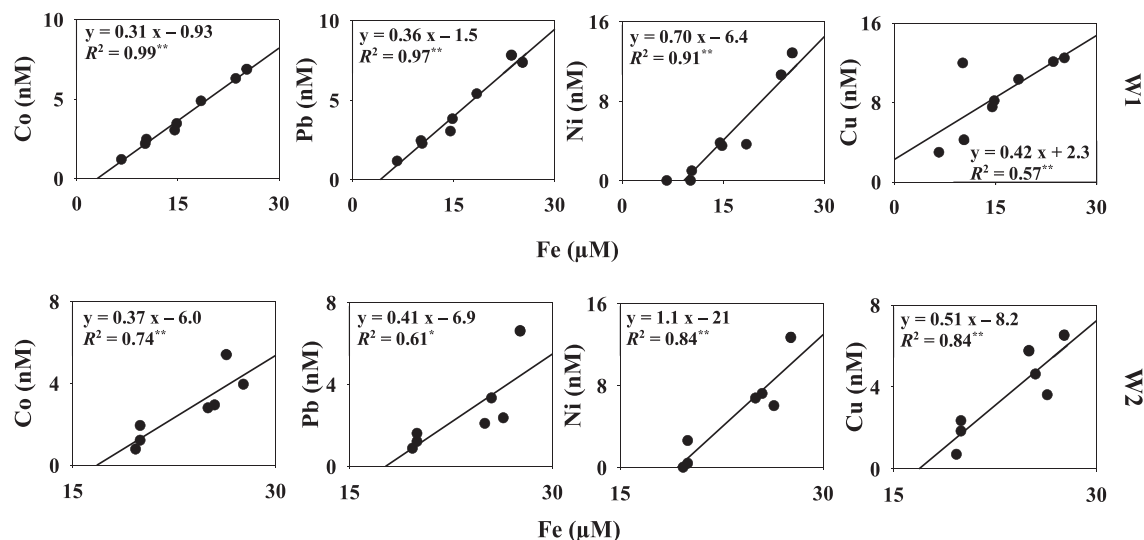
Fig. 5. Correlation analysis between cationic trace metals and Fe in the grey zones (Figs. 2 and 3) at stations W1 and W2 ([**] indicates $p < 0.01$, [*] indicates $p < 0.05$).

cationic trace metals are easily incorporated into FeS and further buried in the sediment. However, FeS can also re-dissolve in porewater releasing the incorporated metals. There are basically two pathways of FeS dissolution: (1) FeS is transported back to the sediment surface for example by bioturbation and then oxidized by O_2, NO_3^- or Fe/Mn oxyhydroxides behaving as potential electron acceptors (Schippers and Jørgensen, 2002). This process is thus not taking place in the grey zone; (2) the other pathway is acidic dissolution by protons, which is caused by acidification of porewater in the sulfidic sediment layer (Widdicombe et al., 2011). A recent discovered process in the deeper, anoxic sediment layer of BCZ sediments, namely electrogenic sulfur oxidation (Malkin et al., 2014), is likely responsible for porewater acidification (van de Velde et al., 2016). The underlying mechanism is electron transport from the anoxic layer to the surface sediment during mineralization of organic matter and is induced by metabolic activity of long filamentous cable bacteria which can be up to several centimeters in length (Pfeffer et al., 2012). Cable bacteria couple the oxidation of sulfide in the anoxic sediment layer (termed anodic sulfide oxidation, ASO),

$$HS^- + 4H_2O \rightarrow SO_4^{2-} + 9H^+ + 8e^- \qquad (2)$$

to the reduction of oxygen near the SWI (termed cathodic oxygen reduction, COR),

$$2O_2 + 8H^+ + 8e^- \rightarrow 4H_2O \qquad (3)$$

To connect these two redox reactions, cable bacteria must transport electrons directly from the deeper layers to the SWI. As a side effect, the spatial decoupling of the oxygen reduction and sulfide oxidation can induce strong pH variations in the porewater (Nielsen et al., 2010). The protons produced during sulfide oxidation can thus dissolve acid sensitive metal sulfides, even if the pH profile is not reflecting strong acidification.

Studies from Motelica-Heino et al. (2003) and Naylor et al. (2004) have shown that stoichiometry ratios of simultaneously released metals

and Fe can be a guide to identify their solid source in sediments. Thus the ratios of cationic trace metal to Fe (TM/Fe, nmol/µmol) in the grey zones at both stations, which are equal to the slopes of the correlation lines in Fig. 5, are summarized in Table 1, and compared with literature values to investigate further if associated cationic trace metals were released during acidic dissolution of FeS in the grey zone. The differences between these ratios at W1 and W2 were generally very small with the smallest found for Pb/Fe (W1/W2 = 88%) and the highest found for Ni/Fe (W1/W2 = 64%). This is a strong indication that the source responsible for the simultaneous release of cationic trace metals and Fe at stations W1 and W2 was the same. Literature values of TM/Fe ratios in FeS in both freshwater (Huerta-Diaz et al., 1993) and coastal surface sediments (Huerta-Diaz and Morse, 1990), at similar depths as in our study, are presented in Table 1. Ni has generally the highest affinity to FeS while Co has the lowest, which agrees with our observation. There is no substantial difference of TM/Fe ratios between freshwater and coastal sediments, suggesting that salinity has a limited influence on the affinity of trace metals to FeS. To better compare these ratios obtained from our study and literature, they were averaged and shown in Table 1. The differences between the averaged ratios in our study (W1 and W2) and those in literature are within a factor of 2 for four metals, proving that the dissolution of FeS was most probably responsible for the simultaneous release of cationic trace metals (Co, Pb, Ni, and Cu) and Fe in the grey zones.

Different from the observed correlation between Co/Pb/Ni/Cu and Fe in the grey zones, Mn, Cd, and Zn showed less affinity to Fe (Figs. 2 and 3). A correlation analysis between Mn/Cd/Zn and Fe was also performed and is shown in Figure S3. Generally, there was no clear correlation between Mn/Cd/Zn and Fe in the grey zones at both stations. Similar to the findings of Huerta-Diaz et al. (1998, 1993), the ratios of Cd/Fe and Zn/Fe in FeS varied significantly between different sediments and there was no distinct correlation between Cd/Zn and Fe. This indicates that Cd and Zn might prefer to form their own sulfides rather

Table 1
The ratios of cationic trace metals to Fe (TM/Fe, nmol/µmol) in the grey zones (Figs. 2 and 3) at stations W1 and W2.

	W1	W2	W1/W2	Average (W1 and W2)	TM/Fe in FeS (freshwater sediments[a])	TM/Fe in FeS (coastal sediments[b])	Average (literature values)
Co/Fe	0.31	0.37	84%	0.34	0.10 – 0.22	0.18	0.17
Pb/Fe	0.36	0.41	88%	0.39	0.42 – 0.74	0.25	0.47
Ni/Fe	0.70	1.1	64%	0.90	0.91 – 1.0	2.1	1.3
Cu/Fe	0.42	0.51	82%	0.47	0.33 – 1.4	0.56	0.76

[a] Huerta-Diaz et al., 1993;
[b] Huerta-Diaz and Morse, 1990.

than to adsorb on or co-precipitate with FeS, which is supported by the finding of Morse and Luther (1999) that Cd and Zn are generally pyritized to only a few percent of their labile fraction, and precipitate as MeS prior to FeS formation and subsequent pyrite formation. Mn has also a different burial process than Fe in sediments and it prefers to precipitate as carbonates instead of sulfides (Jilbert and Slomp, 2013).

4.2. Co-mobilization of P, V, and As with Fe in the BCZ sediment

Oxyanions including P, V, and As were found to co-mobilize with Fe in the blue zones which are close to the SWI (Figs. 2 and 3). Correlation analysis between P/V/As/Mo and Fe in the blue zones were performed and shown in Fig. 6. Significant correlation was found between P/V/As and Fe at both stations but not with Mo and Fe. The correlation coefficients were similar for P, V, and As at both stations with R^2 values around 0.5. The surface of the BCZ sediment is rich in Fe oxyhydroxides (Gao et al., 2012). Similar maximum of Fe in the blue zones were also discovered in other studies in the BCZ sediment (Gao et al., 2009; van de Velde et al., 2016), and attributed to the dissolution of Fe oxyhydroxides. Simultaneous release of Fe and associated oxyanions in sediments has also been documented (Schaller et al., 2000; Slomp et al., 1996). However, different from the constant ratios of TM/Fe in the grey zones at the two stations, the ratios of OA/Fe (Oxyanions/Fe) in the blue zones differed strongly between the two stations (Table 2). A large difference of 370% (W1/W2) was found for As/Fe, while the differences were smaller for P/Fe and V/Fe with 27% and 190% respectively. This suggests that ratios of OA/Fe in Fe oxyhydroxides are not constant. Similar findings were also reported by Breward (2007), who found that P/Fe ratios in Fe oxyhydroxides varied from 0.11 to 0.60 in freshwater sediment, and by Feely et al. (1998) who reported that the ratio of P/Fe in freshly formed ferrihydrite precipitates in Atlantic and Pacific Oceans varied from 0.06 to 0.21. As/Fe ratios varied from 0.07 to 6.92 in 12 Canadian Shield lakes (Vitre et al., 1991) and Neal et al. (1979) found a ratio of As/Fe around 1.1 in North Atlantic deep-sea sediment, while it increased to 5.0 in metalliferous sediment. Strong competition effects between oxyanions for binding on Fe oxyhydroxides is believed to be the reason for the observed wide ranges in OA/Fe ratios. Feely et al. (1998) found that the ratio of P/Fe in Fe oxyhydroxides was positively correlated to the concentration of dissolved phosphate in sea water, while it was negatively correlated with the ratio of V/Fe, demonstrating a strong competing effect between P and V for binding on Fe oxyhydroxides. Rubinos et al. (2011) reported that addition of phosphate (1 mM) significantly increased both the amount and the rate of As released from the sediment which was enriched in Fe oxyhydroxides. This is supported

by our results as the ratios of V/Fe and As/Fe both decreased from station W1 to W2 while the ratio of P/Fe increased (Table 2).

Different from P, V, and As, Mo showed less association with Fe in the blue zones (Fig. 6). In a laboratory experiment, Amrhein et al. (1993) found that Mo was lost from solution under reducing conditions, assuming MoS_2 was formed, and remobilized under oxidizing conditions. Helz et al. (1996) proposed that under reducing conditions, molybdate is converted to thiomolybdate (MoS_4^{2-}) which then binds to Fe, Al, and organic matter phases via sulfur bridging. This suggests that Mo is easier to be immobilized in sediments by forming Mo sulfides, presenting less direct association with Fe. However, considerable concentrations of Mo (500 nM) were still observed in the BCZ sediment, which might result from the dissolution of Mn oxyhydroxides. Scholz et al. (2013) found that there was coupled Mn and Mo delivery to euxinic sediment in the Baltic Sea, which agrees with our findings that Mn and Mo showed similar profiles (Figs. 2 and 3).

4.3. Remobilization mechanisms of cationic trace metals and oxyanions in the BCZ sediment

Evidence obtained from high resolution DGT profiles revealed two mobilization mechanisms of investigated elements in the BCZ sediment: (1) mobilization of cationic trace metals (Co, Pb, Ni, and Cu) are controlled by the dissolution of FeS (deeper, anoxic sediment); (2) mobilization of oxyanions (P, V, and As) are controlled by the dissolution of Fe oxyhydroxides (upper, sub-oxic sediment). Previous studies in the BCZ (Gao et al., 2009) have demonstrated considerable fluxes of Fe, Mn, and trace metals from sediment to overlying water (in the range of 4.4×10^{-5} to 0.10 mmol m^{-2} d^{-1}), but the underlying mechanisms were unknown. Our study shows that dissolution of FeS at depth is an important, hitherto overlooked remobilization mechanism for cationic trace metals. Anthropogenic activities (e.g., dredging and bottom trawling), which frequently take place in the BCZ (van de Velde et al., 2018), can redistribute the sediment, for example bringing FeS minerals to the surface. It will then be oxidatively dissolved by the oxygenated overlying water releasing associated metals into the water column. Van de Velde et al. (2016) reported that the FeS content in the upper 15 cm of the BCZ sediment was around 25 µmol g^{-1}. Hence, based on the average TM/Fe ratios in FeS at stations W1 and W2 (Table 1), respectively 8.5, 9.8, 23, and 12 nmol g^{-1} of Co, Pb, Ni, and Cu could potentially be released into the BCZ water column.

Fe/Mn oxyhydroxide particles and organic matter are considered as two primary carriers of cationic trace metals to sediment (Charriau et al., 2011). In early diagenetic processes, organic matter is quickly
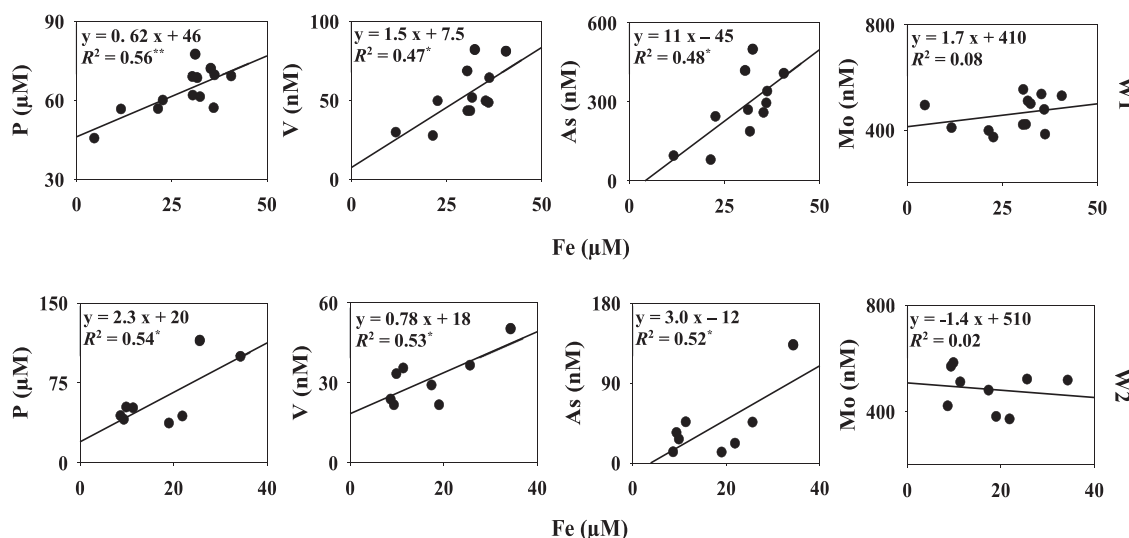

Fig. 6. Correlation analysis between oxyanions and Fe in the blue zones (Figs. 2 and 3) at stations W1 and W2 (** indicates $p < 0.01$, * indicates $p < 0.05$).

Table 2

The ratios of oxyanions to Fe (OA/Fe, nmol/μmol for V and As; μmol/ μmol for P) in the blue zones (Figs. 2 and 3) at stations W1 and W2.

	W1	W2	W1/W2	OA/Fe in Fe oxyhydroxides (freshwater sediments[c, d])	OA/Fe in Fe oxyhydroxides (marine sediments[e, f])
P/Fe	0.62	2.3	27%	0.11 – 0.60[c]	0.06 – 0.21[e]
V/Fe	1.5	0.78	190%	1.9 – 2.5[c]	2.3 – 4.5[e]
As/Fe	11	3.0	370%	0.07 – 6.92[d]	1.1 – 5.0[f]

[c] Breward, 2007;
[d] Vitre et al., 1991;
[e] Feely et al., 1998;
[f] Neal et al., 1979.

degraded as soon as it reaches sediment surface due to bacterial activity, while Fe/Mn oxyhydroxides are subsequently reduced once O_2 is completely consumed. At the same time, cationic trace metals can be simultaneously released into sediment porewater either from the degradation of organic matter or the dissolution of Fe/Mn oxy-hydroxides. However, in our study, no distinct association between cationic trace metals and Fe/Mn oxyhydroxides were found in the BCZ sediment. This suggests that the major input of these metals to the BCZ sediment is from organic matter rather than from Fe/Mn oxyhydroxides. Porewater concentration profiles obtained from routine sediment slicing showed distinct maxima of cationic trace metals at the same station (van de Velde et al., 2016). This indicates that trace metals were released into porewater and were measured by routine porewater analysis but not by DGT. Modeling studies (Charriau et al., 2011; Lourino-Cabana et al., 2014) showed that dissolved cationic trace metals in the BCZ surface sediment are largely complexed by organic ligands, with more than 80% of Cu and Pb presenting in the form of metal-fulvic acids complexes. Strong metal complexes are, however, not measured by the DGT. Moreover, as the pore size of the diffusive gel in DGT device is 10–20 nm (Zhang and Davison, 1999), it is apparently too small to allow those organic compounds to enter. As a result, lower concentrations are measured by DGT compared to those measured by routine porewater analysis. Cationic trace metals are primarily associated with suspended particulate matter (SPM) in the BCZ water column (Gaulier et al., 2019) and enter the sediment in particulate forms. Previous studies (Gaulier et al., 2019; Nolting and Eisma, 1988) have demonstrated that SPM in the BCZ water column is characterized by high POC content (between 3% and 9%) and that cationic trace metal concentrations are significantly ($p < 0.001$) and positively ($0.76 < R^2 < 0.94$) correlated with the variations of POC in SPM. Our finding is also supported by a microcosm study from Gao et al. (2012) who observed higher concentrations of cationic trace metals in the overlying water and higher effluxes of at the SWI that are attributed to the mineralization processes of additional natural phytodetritus.

Oxyanions showed a remobilization mechanism in the BCZ sediment that is different from that of cationic trace metals, and is highly linked to their oxidation state in sediment (Fox and Doner, 2003). P, V, and As all have at least two oxidation states. P(V), V(V), and As(V) are the dominant species in oxygenated water column and are easily adsorbed on Fe/Mn oxyhydroxide particles (Fox and Doner, 2003; Morton et al., 2003), which therefore act as a carrier of oxyanions to the sediment. After entering sediment, Fe/Mn oxyhydroxides are reductively dissolved and associated oxyanions are released into porewater, which is consistent with our observations particularly for Fe. The released As(V) and V(V) are further reduced in sediment porewater mainly due to bacterial activity (Bennett et al., 2012; Tufano et al., 2008). V(III) and V(IV) are two dominant reduced species in porewater which often precipitate as oxides or oxyhydroxides (e.g., V_2O_3, VO(OH), VO_2, and VO(OH)$_2$) and are further buried in deeper sediment (Fox and Doner, 2003). As(III) is the only dominant reduced arsenic species in porewater and is removed from porewater by precipitation with sulfide, which replaces the oxygen atom in the oxyanion complex of As (e.g., AsS, As_2S_3) (Mccreadie et al., 2000). Comparing to As and V, P is more difficult to be reduced and P(V) is still the dominant species in sediment (Han et al., 2013). Instead, it is

prone to form authigenic P-bearing minerals such as apatite (Coelho et al., 2004).

Although our results support the prevailing theory that dissolution of Fe oxyhydroxides is the primary pathway of oxyanions mobilization in sediments, caution is still needed as the correlation coefficients (R^2) between oxyanions and Fe observed in our study were generally around 0.5 (Fig. 6), suggesting that other mechanisms may also be involved. The coincident maxima of P, V, and As observed at −13 cm depth, below the Fe oxyhydroxides dissolution depth, at station W2 (Fig. 3) further supports this conclusion. The simultaneous mobilization of Ca, Mn, and P in Baltic Sea sediment suggests that dissolution of Ca-Mn-carbonate-phosphate is the main pathway of P release from sediment and which may also impact V and As mobilizations (Hermans et al., 2019). Koski-Vahala et al. (2001) found that P equilibrium between Fe-bound P and Al-bound P in sediment regulate P net mobilization to porewater and elevated pH combined with Si enrichment can impose a positive synergistic effect.

5. Conclusion

Two mobilization mechanisms of cationic trace metals and oxyanions in the BCZ sediment were identified using fine scale and multi-element measurements obtained with DGT devices. Fe plays a key role in both mechanisms because the mobilization of cationic trace metals (Co, Pb, Ni, and Cu) is controlled by dissolution of FeS and that of oxyanions (P, V, and As) by dissolution of Fe oxyhydroxides. The association between cationic trace metals and Fe/Mn oxyhydroxides was poor, indicating that the major input of cationic trace metals to the BCZ sediment is related to the settlement of organic matter. While the ratios of TM/Fe in FeS are constant, this is not the case for the ratios of OA/Fe in Fe oxyhydroxides. Strong competition between oxyanions caused a broad range of OA/Fe ratios in Fe oxyhydroxides. Correlation coefficients between oxyanions and Fe were around 0.5, suggesting that other pathways might be involved in the mobilization of these oxyanions. The low degree of association between oxyanions and FeS indicates that in anoxic sediment, the direct formation of oxyanion-sulfide compounds might dominate the diagenetic process of oxyanions instead of their incorporation/association with FeS. These findings provide a fundamental and holistic view of geochemical cycling of cationic trace metals and oxyanions in Belgian coastal sediments.

CRediT authorship contribution statement

Chunyang Zhou: Writing - review & editing, Supervision. **Camille Gaulier:** Investigation, Resources. **Mingyue Luo:** Methodology, Investigation. **Wei Guo:** Validation, Writing - review & editing. **Willy Baeyens:** Writing - review & editing, Supervision. **Yue Gao:** Writing - review & editing, Supervision, Project administration, Funding acquisition.

Declaration of Competing Interest

The authors declare that they have no known competing financial interests or personal relationships that could have appeared to influence

the work reported in this paper.

Acknowledgements

Appendix A. Supplementary data

Supplementary data to this article can be found online at https://doi.org/10.1016/j.envint.2020.106140.

References

Amrhein, C., Mosher, P.A., Brown, A.D., 1993. The effects of redox on Mo, U, B, V, and As solubility in evaporation pond soils. Soil Sci. 155, 249–255. https://doi.org/10.1097/00010694-199304000-00003.

Antipov, A.N., Lyalikova, N.N., Khiznjak, T. V., L'vov, N.P., 1999. Some properties of dissimilatory nitrate reductases lacking molybdenum and molybdenum cofactor. Biochem. C/C BIOKHIMIIA 64, 483–487.

Arsic, M., Teasdale, P.R., Welsh, D.T., Johnston, S.G., Burton, E.D., Hockmann, K., Bennett, W.W., 2018. Diffusive Gradients in Thin Films Reveals Differences in Antimony and Arsenic Mobility in a Contaminated Wetland Sediment during an Oxic-Anoxic Transition. Environ. Sci. Technol. 52, 1118–1127. https://doi.org/10.1021/acs.est.7b03882.

Baeyens, W., Gao, Y., Davison, W., Galceran, J., Leermakers, M., Puy, J., Superville, P.-J., Beguery, L., 2018. In situ measurements of micronutrient dynamics in open seawater show that complex dissociation rates may limit diatom growth. Sci. Rep. 8, 16125–16135. https://doi.org/10.1038/s41598-018-34465-w.

Bennett, W.W., Teasdale, P.R., Panther, J.G., Welsh, D.T., Zhao, H., Jolley, D.F., 2012. Investigating arsenic speciation and mobilization in sediments with DGT and DET: A mesocosm evaluation of oxic-anoxic transitions. Environ. Sci. Technol. 46, 3981–3989. https://doi.org/10.1021/es204484k.

Berner, R.A., 1980. Early diagenesis: A theoretical approach. Princeton University Press.

Borch, T., Masue, Y., K. Kukkadapu, R., Fendorf, S., 2006. Phosphate Imposed Limitations on Biological Reduction and Alteration of Ferrihydrite. Environ. Sci. Technol. 41, 166–172. https://doi.org/10.1021/es060695p.

Breward, N., 2007. Arsenic and presumed resistate trace element geochemistry of the Lincolnshire (UK) sedimentary ironstones, as revealed by a regional geochemical survey using soil, water and stream sediment sampling. Appl. Geochemistry 22, 1970–1993. https://doi.org/10.1016/J.APGEOCHEM.2007.03.058.

Canavan, R.W., Van Cappellen, P., Zwolsman, J.J.G., van den Berg, G.A., Slomp, C.P., 2007. Geochemistry of trace metals in a fresh water sediment: Field results and diagenetic modeling. Sci. Total Environ. 381, 263–279. https://doi.org/10.1016/J.SCITOTENV.2007.04.001.

Charriau, A., Lesven, L., Gao, Y., Leermakers, M., Baeyens, W., Ouddane, B., Billon, G., 2011. Trace metal behaviour in riverine sediments: Role of organic matter and sulfides. Appl. Geochemistry 26, 80–90. https://doi.org/10.1016/J.APGEOCHEM.2010.11.005.

Coelho, J.P., Flindt, M.R., Jensen, H.S., Lillebø, A.I., Pardal, M.A., 2004. Phosphorus speciation and availability in intertidal sediments of a temperate estuary: relation to eutrophication and annual P-fluxes. Estuar. Coast. Shelf Sci. 61, 583–590. https://doi.org/10.1016/J.ECSS.2004.07.001.

Davison, W., Zhang, H., 1994. In situspeciation measurements of trace components in natural waters using thin-film gels. Nature 367, 546–548.

Eady, R.R., 2003. Current status of structure function relationships of vanadium nitrogenase. Coord. Chem. Rev. 237, 23–30. https://doi.org/10.1016/S0010-8545(02)00248-5.

Emerson, S.R., Huested, S.S., 1991. Ocean anoxia and the concentrations of molybdenum and vanadium in seawater. Mar. Chem. 34, 177–196. https://doi.org/10.1016/0304-4203(91)90002-E.

Feely, R.A., Trefry, J.H., Lebon, G.T., German, C.R., 1998. The relationship between P/Fe and V/Fe ratios in hydrothermal precipitates and dissolved phosphate in seawater. Geophys. Res. Lett. 25, 2253–2256. https://doi.org/10.1029/98GL01546.

Fones, G.R., Davison, W., Hamilton-Taylor, J., 2004. The fine-scale remobilization of metals in the surface sediment of the North-East Atlantic. Cont. Shelf Res. 24, 1485–1504. https://doi.org/10.1016/j.csr.2004.05.007.

Fox, P.M., Doner, H.E., 2003. Accumulation, Release, and Solubility of Arsenic, Molybdenum, and Vanadium in Wetland Sediments. J. Environ. Qual. 32, 2428–2435. https://doi.org/10.2134/jeq2003.2428.

Gao, Y., de Brauwere, A., Elskens, M., Croes, K., Baeyens, W., Leermakers, M., 2013. Evolution of trace metal and organic pollutant concentrations in the Scheldt River Basin and the Belgian Coastal Zone over the last three decades. J. Mar. Syst. 128, 52–61. https://doi.org/10.1016/j.jmarsys.2012.04.002.

Gao, Y., Leermakers, M., Pede, A., Magnier, A., Sabbe, K., Lourino Cabana, B., Billon, G., Baeyens, W., Gillan, D.C., 2012. Response of diffusive equilibrium in thin films (DET) and diffusive gradients in thin films (DGT) trace metal profiles in sediments to phytodetritus mineralisation. Environ. Chem. 9, 41–47. https://doi.org/10.1071/EN11075.

Gao, Y., Lesven, L., Gillan, D., Sabbe, K., Billon, G., De Galan, S., Elskens, M., Baeyens, W., Leermakers, M., 2009. Geochemical behavior of trace elements in subtidal marine sediments of the Belgian coast. Mar. Chem. 117, 88–96. https://doi.org/10.1016/j.marchem.2009.05.002.

Gao, Y., van de Velde, S., Williams, P.N., Baeyens, W., Zhang, H., 2015. Two-dimensional images of dissolved sulfide and metals in anoxic sediments by a novel diffusive gradients in thin film probe and optical scanning techniques. TrAC - Trends Anal. Chem. 66, 63–71. https://doi.org/10.1016/j.trac.2014.11.012.

Gao, Y., Zhou, C., Gaulier, C., Bratkic, A., Galceran, J., Puy, J., Zhang, H., Leermakers, M., Baeyens, W., 2019. Labile trace metal concentration measurements in marine environments: From coastal to open ocean areas. TrAC Trends Anal. Chem. 116, 92–101. https://doi.org/10.1016/J.TRAC.2019.04.027.

Gaulier, C., Zhou, C., Guo, W., Bratkic, A., Superville, P.-J., Billon, G., Baeyens, W., Gao, Y., 2019. Trace metal speciation in North Sea coastal waters. Sci. Total Environ. 692, 701–712. https://doi.org/10.1016/J.SCITOTENV.2019.07.314.

Gendron, A., Silverberg, N., Sundby, B., Lebel, J., 1986. Early diagenesis of cadmium and cobalt in sediments of the Laurentian Trough. Geochim. Cosmochim. Acta 50, 741–747. https://doi.org/10.1016/0016-7037(86)90350-9.

Gillan, D.C., Pede, A., Sabbe, K., Gao, Y., Leermakers, M., Baeyens, W., Louriño Cabana, B., Billon, G., 2012. Effect of bacterial mineralization of phytoplankton-derived phytodetritus on the release of arsenic, cobalt and manganese from muddy sediments in the Southern North Sea. A microcosm study. Sci. Total Environ. 419, 98–108. https://doi.org/10.1016/J.SCITOTENV.2011.12.034.

Guan, D.X., Williams, P.N., Luo, J., Zheng, J.L., Xu, H.C., Cai, C., Ma, L.Q., 2015. Novel precipitated zirconia-based DGT technique for high-resolution imaging of oxyanions in waters and sediments. Environ. Sci. Technol. 49, 3653–3661. https://doi.org/10.1021/es505424m.

Gustafsson, J.P., 2003. Modelling molybdate and tungstate adsorption to ferrihydrite. Chem. Geol. 200, 105–115. https://doi.org/10.1016/S0009-2541(03)00161-X.

Halpern, B.S., Walbridge, S., Selkoe, K.A., Kappel, C.V., Micheli, F., D'Agrosa, C., Bruno, J.F., Casey, K.S., Ebert, C., Fox, H.E., Fujita, R., Heinemann, D., Lenihan, H.S., Madin, E.M.P., Perry, M.T., Selig, E.R., Spalding, M., Steneck, R., Watson, R., 2008. A global map of human impact on marine ecosystems. Science. 319, 948–952. https://doi.org/10.1126/science.1149345.

Han, C., Geng, J., Ren, H., Gao, S., Xie, X., Wang, X., 2013. Phosphite in Sedimentary Interstitial Water of Lake Taihu, a Large Eutrophic Shallow Lake in China. Environ. Sci. Technol. 47, 5679–5685. https://doi.org/10.1021/es305297y.

Helz, G.R., Miller, C.V., Charnock, J.M., Mosselmans, J.F.W., Pattrick, R.A.D., Garner, C.D., Vaughan, D.J., 1996. Mechanism of molybdenum removal from the sea and its concentration in black shales: EXAFS evidence. Geochim. Cosmochim. Acta 60, 3631–3642. https://doi.org/10.1016/0016-7037(96)00195-0.

Hermans, M., Lenstra, W.K., van Helmond, N.A.G.M., Behrends, T., Egger, M., Séguret, M.J.M., Gustafsson, E., Gustafsson, B.G., Slomp, C.P., 2019. Impact of natural re-oxygenation on the sediment dynamics of manganese, iron and phosphorus in a euxinic Baltic Sea basin. Geochim. Cosmochim. Acta 246, 174–196. https://doi.org/10.1016/J.GCA.2018.11.033.

Howarth, R.W., Cole, J.J., 1985. Molybdenum availability, nitrogen limitation, and phytoplankton growth in natural waters. Science (80-.). 229, 653–655. https://doi.org/10.1126/science.229.4714.653.

Huerta-Diaz, M.A., Carignan, R., Tessier, A., 1993. Measurement of Trace Metals Associated with Acid Volatile Sulfides and Pyrite in Organic Freshwater Sediments. Environ. Sci. Technol. 27, 2367–2372. https://doi.org/10.1021/es00048a009.

Huerta-Diaz, M.A., Morse, J.W., 1990. A quantitative method for determination of trace metal concentrations in sedimentary pyrite. Mar. Chem. 29, 119–144. https://doi.org/10.1016/0304-4203(90)90009-2.

Huerta-Diaz, M.A., Tessier, A., Carignan, R., 1998. Geochemistry of trace metals associated with reduced sulfur in freshwater sediments. Appl. Geochemistry 13, 213–233. https://doi.org/10.1016/S0883-2927(97)00060-7.

Jilbert, T., Slomp, C.P., 2013. Iron and manganese shuttles control the formation of authigenic phosphorus minerals in the euxinic basins of the Baltic Sea. Geochim. Cosmochim. Acta 107, 155–169. https://doi.org/10.1016/j.gca.2013.01.005.

Johnson, K.S., Stout, P.M., Berelson, W.M., Sakamoto-Arnold, C.M., 1988. Cobalt and copper distributions in the waters of Santa Monica Basin, California. Nature 332, 527–530. https://doi.org/10.1038/332527a0.

Kay, J.T., Conklin, M.H., Fuller, C.C., O'Day, P.A., 2001. Processes of nickel and cobalt uptake by a manganese oxide forming sediment in Pinal Creek, Globe mining district. Arizona. Environ. Sci. Technol. 35, 4719–4725. https://doi.org/10.1021/es010514d.

Koski-Vähälä, J., Hartikainen, H., Tallberg, P., 2001. Phosphorus Mobilization from Various Sediment Pools in Response to Increased pH and Silicate Concentration. J. Environ. Qual. 30, 546–552. https://doi.org/10.2134/jeq2001.302546x.

Leermakers, M., Gao, Y., Gabelle, C., Lojen, S., Ouddane, B., Wartel, M., Baeyens, W., 2005. Determination of high resolution pore water profiles of trace metals in sediments of the Rupel River (Belgium) using DET (diffusive equilibrium in thin films) and DGT (diffusive gradients in thin films) techniques. Water. Air. Soil Pollut. 166, 265–286. https://doi.org/10.1007/s11270-005-6671-7.

Lohrer, A.M., Wetz, J.J., 2003. Dredging-induced nutrient release from sediments to the water column in a southeastern saltmarsh tidal creek. Mar. Pollut. Bull. 46, 1156–1163. https://doi.org/10.1016/S0025-326X(03)00167-X.

Lourino-Cabana, B., Billon, G., Lesven, L., Sabbe, K., Gillan, D.C., Gao, Y., Leermakers, M., Baeyens, W., 2014. Monthly variation of trace metals in North Sea sediments: From experimental data to modeling calculations. Mar. Pollut. Bull. 87, 237–246. https://doi.org/10.1016/j.marpolbul.2014.07.053.

Maia, L.B., Moura, J.J.G., 2015. Nitrite reduction by molybdoenzymes: A new class of nitric oxide-forming nitrite reductases. J. Biol. Inorg. Chem. 20, 403–433. https://doi.org/10.1007/s00775-014-1234-2.

Malkin, S.Y., Rao, A.M.F., Seitaj, D., Vasquez-Cardenas, D., Zetsche, E.M., Hidalgo-Martinez, S., Boschker, H.T.S., Meysman, F.J.R., 2014. Natural occurrence of microbial sulphur oxidation by long-range electron transport in the seafloor. ISME J. 8, 1843–1854. https://doi.org/10.1038/ismej.2014.41.

Mccreadie, H., Blowes, D.W., Ptacek, C.J., Jambor, J.L., 2000. Influence of reduction reactions and solid-phase composition on porewater concentrations of arsenic. Environ. Sci. Technol. 34, 3159–3166. https://doi.org/10.1021/es991194p.

Morel, F.M.M., Milligan, A.J., Saito, M.A., 2006. Marine bioinorganic chemistry: the role of trace metals in the oceanic cycles of major nutrients. In: Elderfield, H. (Ed.), The Oceans and Marine Geochemistry. Elsevier Ltd., pp. 113–140

Morel, F.M.M., Price, N.M., 2003. The Biogeochemical Cycles of Trace Metals in the Oceans. Science 300, 944–947. https://doi.org/10.1126/science.1083545.

Morel, F.M.M., Reinfelder, J.R., Roberts, S.B., Chamberlain, C.P., Lee, J.G., Yee, D., 1994. Zinc and carbon co-limitation of marine phytoplankton. Nature 369, 740–742. https://doi.org/10.1038/369740a0.

Morse, J.W., Luther, G.W., 1999. Chemical influences on trace metal-sulfide interactions in anoxic sediments. Geochim. Cosmochim. Acta 63, 3373–3378.

Morton, S.C., Glindemann, D., Edwards, M.A., 2003. Phosphates, phosphites, and phosphides in environmental samples. Environ. Sci. Technol. 37, 1169–1174. https://doi.org/10.1021/es020738b.

Motelica-Heino, M., Naylor, C., Zhang, H., Davison, W., 2003. Simultaneous release of metals and sulfide in lacustrine sediment. Environ. Sci. Technol. 37, 4374–4381. https://doi.org/10.1021/es030035+.

Muylaert, K., Gonzales, R., Franck, M., Lionard, M., Van der Zee, C., Cattrijsse, A., Sabbe, K., Chou, L., Vyverman, W., 2006. Spatial variation in phytoplankton dynamics in the Belgian coastal zone of the North Sea studied by microscopy, HPLC-CHEMTAX and underway fluorescence recordings. J. Sea Res. 55, 253–265. https://doi.org/10.1016/j.seares.2005.12.002.

Naylor, C., Davison, W., Motelica-Heino, M., Van Den Berg, G.A., Van Der Heijdt, L.M., 2004. Simultaneous release of sulfide with Fe, Mn, Ni and Zn in marine harbour sediment measured using a combined metal/sulfide DGT probe. Sci. Total Environ. 328, 275–286. https://doi.org/10.1016/j.scitotenv.2004.02.008.

Neal, C., Elderfield, H., Chester, R., 1979. Arsenic in sediments of the North Atlantic Ocean and the Eastern Mediterranean Sea. Mar. Chem. 7, 207–219. https://doi.org/10.1016/0304-4203(79)90040-9.

Nielsen, L.P., Risgaard-Petersen, N., Fossing, H., Christensen, P.B., Sayama, M., 2010. Electric currents couple spatially separated biogeochemical processes in marine sediment. Nature 463, 1071–1074. https://doi.org/10.1038/nature08790.

Nolting, R.F., Eisma, D., 1988. Elementary composition of suspended particulate matter in the North Sea. Netherlands J. Sea Res. 22, 219–236. https://doi.org/10.1016/0077-7579(88)90026-9.

Pfeffer, C., Larsen, S., Song, J., Dong, M., Besenbacher, F., Meyer, R.L., Kjeldsen, K.U., Schreiber, L., Gorby, Y.A., El-Naggar, M.Y., Leung, K.M., Schramm, A., Risgaard-Petersen, N., Nielsen, L.P., 2012. Filamentous bacteria transport electrons over centimetre distances. Nature 491, 218–221. https://doi.org/10.1038/nature11586.

Rehder, D., 2000. Vanadium nitrogenase. J. Inorg. Biochem. 80, 133–136. https://doi.org/10.1016/S0162-0134(00)00049-0.

Robertson, E.K., Roberts, K.L., Burdorf, L.D.W., Cook, P., Thamdrup, B., 2016. Dissimilatory nitrate reduction to ammonium coupled to Fe(II) oxidation in sediments of a periodically hypoxic estuary. Limnol. Oceanogr. 61, 365–381. https://doi.org/10.1002/lno.10220.

Rubinos, D.A., Iglesias, L., Díaz-Fierros, F., Barral, M.T., 2011. Interacting Effect of pH, Phosphate and Time on the Release of Arsenic from Polluted River Sediments (Anllóns River, Spain). Aquat. Geochemistry 17, 281–306. https://doi.org/10.1007/s10498-011-9135-2.

Schaller, T., Morford, J., Emerson, S.R., Feely, R.A., 2000. Oxyanions in metalliferous sediments: tracers for paleoseawater metal concentrations? Geochim. Cosmochim. Acta 64, 2243–2254. https://doi.org/10.1016/S0016-7037(99)00443-3.

Schippers, A., Jørgensen, B.B., 2002. Biogeochemistry of pyrite and iron sulfide oxidation in marine sediments. Geochim. Cosmochim. Acta 66, 85–92. https://doi.org/10.1016/S0016-7037(01)00745-1.

Scholz, F., McManus, J., Sommer, S., 2013. The manganese and iron shuttle in a modern euxinic basin and implications for molybdenum cycling at euxinic ocean margins. Chem. Geol. 355, 56–68. https://doi.org/10.1016/J.CHEMGEO.2013.07.006.

Slomp, C.P., Van der Gaast, S.J., Van Raaphorst, W., 1996. Phosphorus binding by poorly crystalline iron oxides in North Sea sediments. Mar. Chem. 52, 55–73. https://doi.org/10.1016/0304-4203(95)00078-X.

Stockdale, A., Davison, W., Zhang, H., 2010a. 2D simultaneous measurement of the oxyanions of P, V, As, Mo, Sb, W and U. J. Environ. Monit. 12, 981–984. https://doi.org/10.1039/b925627j.

Stockdale, A., Davison, W., Zhang, H., 2009. Micro-scale biogeochemical heterogeneity in sediments: A review of available technology and observed evidence. Earth-Science Rev. 92, 81–97. https://doi.org/10.1016/j.earscirev.2008.11.003.

Stockdale, A., Davison, W., Zhang, H., Hamilton-Taylor, J., 2010b. The association of Cobalt with Iron and Manganese (Oxyhydr)oxides in marine sediment. Aquat. Geochemistry 16, 575–585. https://doi.org/10.1007/s10498-010-9092-1.

Sullivan, K.A., Aller, R.C., 1996. Diagenetic cycling of arsenic in Amazon shelf sediments. Geochim. Cosmochim. Acta 60, 1465–1477. https://doi.org/10.1016/0016-7037(96)00040-3.

Sulu-Gambari, F., Roepert, A., Jilbert, T., Hagens, M., Meysman, F.J.R., Slomp, C.P., 2017. Molybdenum dynamics in sediments of a seasonally-hypoxic coastal marine basin. Chem. Geol. 466, 627–640. https://doi.org/10.1016/J.CHEMGEO.2017.07.015.

Teasdale, P.R., Hayward, S., Davison, W., 1999. In situ, High-Resolution Measurement of Dissolved Sulfide Using Diffusive Gradients in Thin Films with Computer-Imaging Densitometry. Anal. Chem. 71, 2186–2191. https://doi.org/10.1021/ac981329u.

Thamdrup, B., Fossing, H., Jorgensen, B.B., 1994. Manganese, iron and sulfur cycling in a coastal marine sediment, Aarhus Bay. Denmark. Geochim. Cosmochim. Acta 58, 5115–5129.

Tufano, K.J., Reyes, C., Saltikov, C.W., Fendorf, S., 2008. Reductive processes controlling arsenic retention: Revealing the relative importance of iron and arsenic reduction. Environ. Sci. Technol. 42, 8283–8289. https://doi.org/10.1021/es801059s.

van de Velde, S., Callebaut, I., Gao, Y., Meysman, F.J.R., 2017. Impact of electrogenic sulfur oxidation on trace metal cycling in a coastal sediment. Chem. Geol. 452, 9–23. https://doi.org/10.1016/J.CHEMGEO.2017.01.028.

van de Velde, S., Lesven, L., Burdorf, L.D.W., Hidalgo-Martinez, S., Geelhoed, J.S., Van Rijswijk, P., Gao, Y., Meysman, F.J.R., 2016. The impact of electrogenic sulfur oxidation on the biogeochemistry of coastal sediments: A field study. Geochim. Cosmochim. Acta 194, 211–232. https://doi.org/10.1016/j.gca.2016.08.038.

van de Velde, S., Van Lancker, V., Hidalgo-Martinez, S., Berelson, W.M., Meysman, F.J.R., 2018. Anthropogenic disturbance keeps the coastal seafloor biogeochemistry in a transient state. Sci. Rep. 8, 5582–5591. https://doi.org/10.1038/s41598-018-23925-y.

Vitre, R. De, Belzile, N., Tessier, A., 1991. Speciation and adsorption of arsenic on diagenetic iron oxyhydroxides. Limnol. Oceanogr. 36, 1480–1485. https://doi.org/10.4319/lo.1991.36.7.1480.

Wang, D., Sañudo Wilhelmy, S.A., 2009. Vanadium speciation and cycling in coastal waters. Mar. Chem. 117, 52–58. https://doi.org/10.1016/J.MARCHEM.2009.06.001.

Widdicombe, S., Spicer, J.I., Kitidis, V., 2011. Effects of ocean acidification on sediment fauna. In: Gattuso, J.-.P., Hansson, L. (Eds.), Ocean Acidification. Oxford University Press, pp. 176–191.

Zhang, H., Davison, W., 1999. Diffusional characteristics of hydrogels used in DGT and DET techniques. Anal. Chim. Acta 398, 329–340. https://doi.org/10.1016/S0003-2670(99)00458-4.

Zhang, H., Davison, W., Miller, S., Tych, W., 1995. In situ high resolution measurements of fluxes of Ni, Cu, Fe, and Mn and concentrations of Zn and Cd in porewaters by DGT. Geochim. Cosmochim. Acta 59, 4181–4192.

Zhang, H., Davison, W., Mortimer, R.J.G., Krom, M.D., Hayes, P.J., Davies, I.M., 2002. Localised remobilization of metals in a marine sediment. Sci. Total Environ. 296, 175–187.

Zhou, C., van de Velde, S., Baeyens, W., Gao, Y., 2018. Comparison of Chelex based resins in diffusive gradients in thin-film for high resolution assessment of metals. Talanta 186, 397–405. https://doi.org/10.1016/j.talanta.2018.04.085.